Tensile Deformation of Oriented Poly(ε-caprolactone) and Its Miscible Blends with Poly(vinyl methyl ether)

Zhiyong Jiang[1,], Yaotao Wang[1], Lianlian Fu[1], Ben Whiteside[2], John Wyborn[2], Keith Norris[2], Zhonghua Wu[3], Phil Coates[2,*], and Yongfeng Men[1]*

1. State Key Laboratory of Polymer Physics and Chemistry, Changchun Institute of Applied Chemistry, Chinese Academy of Sciences, Renmin Street 5625, 130022 Changchun, P.R. China

2. School of Engineering, Design and Technology, Uviversity of Bradford, Bradford BD7 1DP, UK

3. BSRF, Institute of High Energy Physics, Chinese Academy of Sciences, 100049 Beijing, P.R. China

[*]Corresponding authors. E-mail addresses: jiangzhy@ciac.jl.cn (Z. Jiang); p.d.coates@bradford.ac.uk (P. Coates)

Abstract

The structural evolution of micro-molded poly(ε-caprolactone) (PCL) and its miscible blends with noncrystallizable poly(vinyl methyl ether) (PVME) at the nanoscale was investigated as a function of deformation ratio and blend composition using in situ synchrotron small-angle X-ray scattering (SAXS) and scanning SAXS techniques. It was found that the deformation mechanism of the oriented samples shows a general scheme for the process of tensile deformation: crystal block slips within the lamellae occur at small deformations followed by a stress-induced fragmentation and recrystallization process along the drawing direction at a critical strain where the average thickness of the crystalline lamellae remains essentially constant during stretching. The value of the critical strain depends on the amount of the amorphous component incorporated in the blends, which could be traced back to the lower modulus of the entangled amorphous phase and, therefore, the reduced network stress acting on the crystallites upon addition of PVME. When stretching beyond the critical strain the slippage of the fibrils (stacks of newly formed lamellae) past each other takes place resulting in a relaxation of stretched interlamellar amorphous chains. Because of deformation-induced introduction of the amorphous PVME into the interfibrillar regions in the highly oriented blends, the interactions between fibrils becomes stronger upon further deformation and thus impeding sliding of the fibrils to some extent leading finally to less contraction of the interlamellar amorphous layers compared to the pure PCL.

1. Introduction

Semicrystalline polymeric materials are often processed in the entangled molten phase by various industrial shaping operations, including injection molding, extrusion, and film blowing. In most cases, these processes cause orientation and elongation of randomly coiled molecular chain segments in a melt and thus substantially affect the subsequent crystallization kinetics, resulting in different structures than the isotropic spherulitic morphologies which evolve under quiescent crystallization conditions.[1,2] Generally, the injection molded samples of various semicrystalline polymers exhibit a clear multiphase structure of skin layers and core, and furthermore, the relative weights of the two contributions change with the polymer melt properties and molding conditions.[3-10] To a large extent, the mechanical properties of semicrystalline polymers are related to the microstructure and morphology.[11-14] It is therefore anticipated that the macroscopic deformation behavior and physical properties will be affected by the heterogeneous nature of molded samples. In fact, the effect of the crystalline structure and orientation on the mechanical behavior of polymers has been reported by numerous investigations.[3,15-18]

Being composed of the interpenetrating networks built up by both crystalline lamellae and the entangled amorphous polymeric chains in between, semicrystalline polymers always exhibit a complex deformation behavior under tensile deformation.[1,19-23] The behavior of the polymers during stretching is generally influenced by both the crystalline and the amorphous phases.[12,24-28] The small-deformation properties are found to depend only on the nature of crystalline lamellae; whereas the ultimate properties are dominated

by the entangled amorphous network.[11,13,25] Poly(ε-caprolactone) (PCL) is a biodegradable polymer, which can form homogeneous mixtures in the melt and solution with a wealth of other noncrystallizable compounds, including poly(vinyl methyl ether) (PVME),[24,29] poly(styrene-co-acrylonitrile),[30,31] and poly(vinyl chloride).[32,33] PCL is, therefore, a natural candidate to investigate the effect of blending on the mechanical properties and deformation behavior, thus providing new insight into the role of the entangled amorphous phase in the tensile deformation of semicrystalline polymers. A variety of reports have addressed deformation characteristics and orientational behavior in PCL-based miscible blends under a tensile load utilizing true stress-strain measurements and infrared spectroscopy.[24,25,34,35] However, the structural and molecular parameters involved in the tensile deformation of PCL-based miscible mixtures are not yet completely understood, mainly because of the deficit of structural and morphological information at the molecular and nanometric length scales during stretching. Hence, it is essential to probe into the micro- and nanostructural development, which occurs during the mechanical deformation of the material, to gain further insight into the molecular mechanisms of tensile deformation and to provide possible routes for improvement of the material.

In the present work, we focused on the influence of the entangled amorphous phase and the lamellar orientation on the structural evolution of PCL and its blends at the lamellar length scale using in situ synchrotron small-angle X-ray scattering (SAXS) and scanning SAXS techniques. For this purpose, samples with different entanglement density of the

amorphous phase were obtained via incorporation of a noncrystallizable component PVME into the semicrystalline polymer PCL. Afterwards, a micro-molding technique was employed to create oriented structures in the miscible blends. As it turned out, new insight into the cooperative deformational behavior being mediated via slippage of fibrils was gained at high elongations. As a consequence of deformation-induced phase separation in the blends, this slippage was suppressed to some extent due to strong interactions between fibrils on a mesoscopic scale after lamellar-to-fibrillar transition.

2. Experimental Section

The PCL used in this study was purchased from Aldrich Chemical Co. and had a number-averaged molecular weight of M_n=80 000 g/mol. The amorphous polymer PVME with a weight-averaged molecular weight of M_w=20 000 g/mol and a polydispersity index of 2.5 was obtained in the state of 50 wt% in water. PCL/PVME blends in different proportions were prepared in a tetrahydrofuran solution. The THF solvent was evaporated at room temperature by first keeping samples for 24 h in air and then placing the blends in a vacuum oven for three days. After sufficient evaporation of the solvent, samples for the measurements were molded into dumbbell-shaped strips with a dimension of $25 \times 2.0 \times 1.0$ mm^3 using a Battenfeld Microsystem50 machine. The melt temperature and the mold temperature were preset at 100 ^{o}C and 30 ^{o}C, respectively. In addition, the injection velocity was varied from 100 mm/s, 300 mm/s and 900 mm/s with the

objectives of evaluating the effect of micro-molding process conditions on the crystalline morphology and mechanical behavior of the as-received product.

In situ synchrotron SAXS measurements were performed at the beamline 1W2A at BSRF, Beijing, China, with the wavelength of synchrotron X-ray radiation being 0.154 nm. A portable tensile testing machine (TST350, Linkam, UK) was employed to carry out uniaxial tensile deformation and was mounted onto a two-dimensional translational stage at the beamline with a sample to detector distance of 1697 mm. At this distance the effective scattering vector q ($q = (4\pi \sin\theta)/\lambda$, where 2θ is the scattering angle and λ the wavelength) range is 0.20-1.60 nm^{-1}. The size of the X-ray beam at the sample position was 1.4 × 0.2 mm^2. The incident X-ray beam was first illuminated at the middle of the horizontally placed sample bar. The samples were then stretched along the flow direction at a constant crosshead speed of 0.01 mm/s at room temperature, and SAXS data were recorded with an exposure time of 30 s by a Mar165 CCD detector (resolution: 2048 × 2048) after each step was completed. Meanwhile, optical images of the deformed samples were recorded with the aid of a camera in order to measure the true strain at the position of the X-ray beam. The cycle of stretching and subsequent data acquisition was repeated until the neck region had propagated over the entire gauge length of the sample. Additionally, in order to explore the influence of the structural inhomogeneity on the deformation behavior of micro-molded samples, the structural evolution of the core and skin layers was probed as a function of strain using a scanning small-angle X-ray scattering technique on a modified Xeuss system of Xenocs, France. The setup was

equipped with a GeniX 3D Cu Ultra Low divergence (ULD) beam delivery system. The wavelength of the X-ray radiation was 0.154 nm. The beam size at the sample position was 0.1 × 0.1 mm^2 realized by a prolonged (2.4 m) two slits collimation system. The micro-molded samples were stretched along the injection direction at a constant crosshead speed of 0.01 mm/s at room temperature with a tensile testing device (TST350, Linkam, UK) until neck propagation occurred over a large portion of the samples. The drawn samples were not fixed at their two ends in the stretched state when they were taken out of the tensile machine. A strip of 0.5 mm width was then cut from the middle of the prestretched sample along the stretching direction and was mounted onto a two-dimensional translational stage at the beamline with a sample to detector distance of 1062 mm. The strip was moved stepwise in such a way that the X-ray beam scanned over the core and skin layers, respectively. SAXS patterns were collected at several elongation ratios with an exposure time of 3600 s by a Pilatus 100K detector (resolution: 487 × 195). The SAXS data were calibrated for background scattering and normalized with respect to the primary beam intensity. Changes in scattering intensities due to varying sample thicknesses were corrected by measuring sample adsorption using ionization chambers before and after the sample and by performing the corresponding data correction.

The distribution of flow-induced oriented structures in the middle of micro-molded samples was analyzed before deformation by microfocus wide-angle X-ray scattering (WAXS) technique. Synchrotron WAXS measurements of this set of molded samples were performed at the beamline BL15U1 at SSRF, Shanghai, China with the wavelength

of X-ray being 0.06199 nm. The primary X-ray beam with a beam spot of 4.0 × 4.0 μm^2 was first positioned at the middle of the dumbbell-shaped sample bar, and the samples were then moved stepwise in such a way that the X-ray beam scanned over the width at a step length of 20 μm. On the other hand, samples of 0.5 mm width were cut from the middle of the molded specimens along the injection direction, and WAXS diagrams were recorded by scanning over half the thickness of the rectangular strips with steps of 10 μm. Each WAXS pattern was collected with an accumulation time of 2 s by a Mar165 CCD detector (resolution: 2048 × 2048) at a sample to detector distance of 187 mm.

Assuming a constant volume during the elongation, the Hencky measure of the strain ε_H was used as a measure for the deformation. This is defined as

$$\varepsilon_H = 2 \ln \frac{b_0}{b} \qquad (1)$$

where b_0 and b represent the widths of the undeformed and deformed areas located at specific spots on the samples. Following this equation, true stress-strain curves were obtained at a constant crosshead speed of 0.01 mm/s by an imaging of the neck profile and a recording of the applied force.

To obtain further information on the samples, differential scanning calorimetry (DSC) measurements were conducted on the middle of the micro-molded specimens before stretching. A DSC1 Star^e System (Mettler Toledo Instruments), which had been calibrated for temperature and melting enthalpy by using indium as a standard, was used during the experiments with a heating rate of 10 K/min. In addition, polarized optical

microscopy (Zeiss Axio Imager A2m, Carl Zeiss, Germany) was employed to visualize the thickness of oriented skin layers. Cross sections were prepared from the middle of micro-molded samples, and were observed between crossed polars at 45^{o} and 90^{o} with respect to the injection direction.

3. Results and Discussion

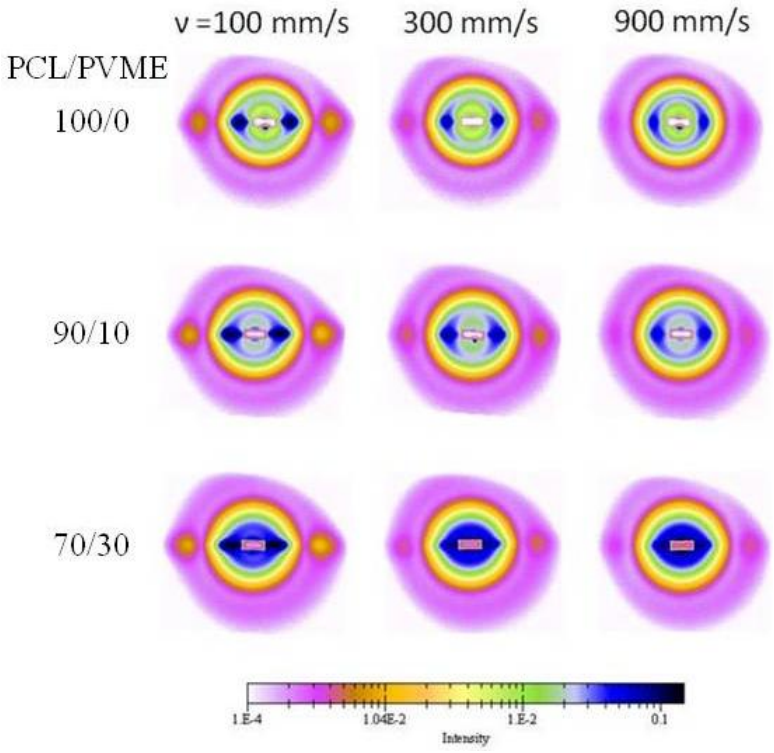

Figure 1. Small-angle X-ray scattering patterns of PCL/PVME blends micro-molded at different injection velocities before tensile deformation. The shear flow direction is horizontal. The effective q range of SAXS diagrams is 0.20-1.60 nm^{-1}.

3.1. Structure Characterization before Deformation. Before considering the microstructural evolution under tensile deformation, we present the crystalline structures of micro-molded blends at different injection velocities. Figure 1 shows SAXS patterns of the pure PCL and its blends with PVME as a function of injection velocity. It is clear that the SAXS patterns for the micro-molded blends exhibit a moderately anisotropic scattering intensity distribution with scattering peaks aligned along the shear flow direction, reflecting the presence of residual lamellar orientation induced during the injection molding. As it appears, there is an overall increase in the scattering intensity with increasing concentration of PVME after micro-molding. This finding supports the fact that the amorphous polymer PVME was introduced into the amorphous phase of PCL and thus leading to an increase of the electron density difference between the crystalline lamellae and the amorphous layers in between. Furthermore, both the PVME content and the injection velocity have a significant effect on the level of crystalline orientation, as evidenced by the azimuthal widths of the scattering arcs. However, it is difficult to calculate the degree of orientation based on a single meridional SAXS spot, as the size broadening affects the level of correction and superimposes on the angular spread when the orientation is high.[36]

In an effort to evaluate the distribution of oriented structures, the 2D WAXS images were recorded at different positions along the width of the micro-molded pure PCL samples as given in Figure 2. The resultant azimuthal scans of the intensity distribution of the 110-reflection (Figure 3) demonstrate that the sample micro-molded at 100 mm/s

exhibits a higher level of orientation at a position in the middle of the sample as compared to the one molded at 900 mm/s. This observation can be tentatively explained in the following way. A higher injection speed has the consequence that there is less time for the material to cool to form a frozen layer during the filling phase, restricting the thickness of the shear regions in the component and resulting in a thicker core region with a low degree of orientation. Accordingly, the average value of crystalline orientation that exists through the bulk of the sample is lower for samples micro-molded at higher injection velocities, as evidenced by a distinct reduction in the intensity maximum observed in azimuthal intensity distributions at an injection speed of 900 mm/s. In addition, at higher filling rates, wall slip can occur which reduces the level of shear stress and therefore the degree of orientation.

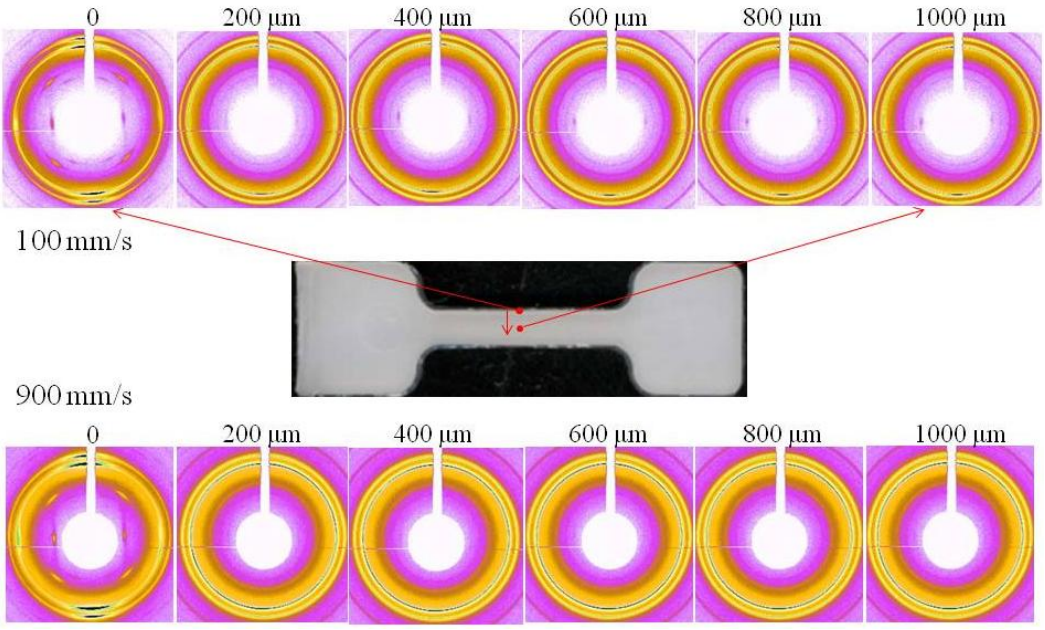

Figure 2. Selected wide-angle X-ray scattering patterns of micro-molded pure PCL at 100 (top) and 900 mm/s (bottom) measured as a function of distance from the sample

edge as indicated on the graph. The effective q range of WAXS diagrams is 2.75-38.97 nm^{-1}.

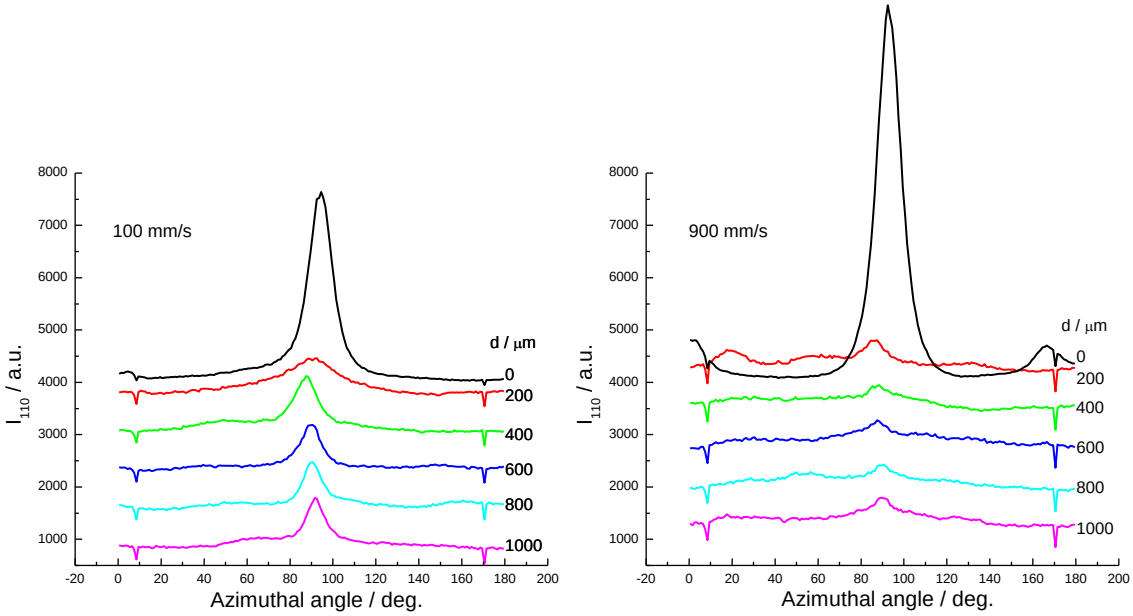

Figure 3. Azimuthal intensity distribution of the 110-reflection measured for the pure PCL sample micro-molded at 100 (left) and 900 mm/s (right) as a function of distance from the edge. Only one half of the data is presented for the sake of clarity.

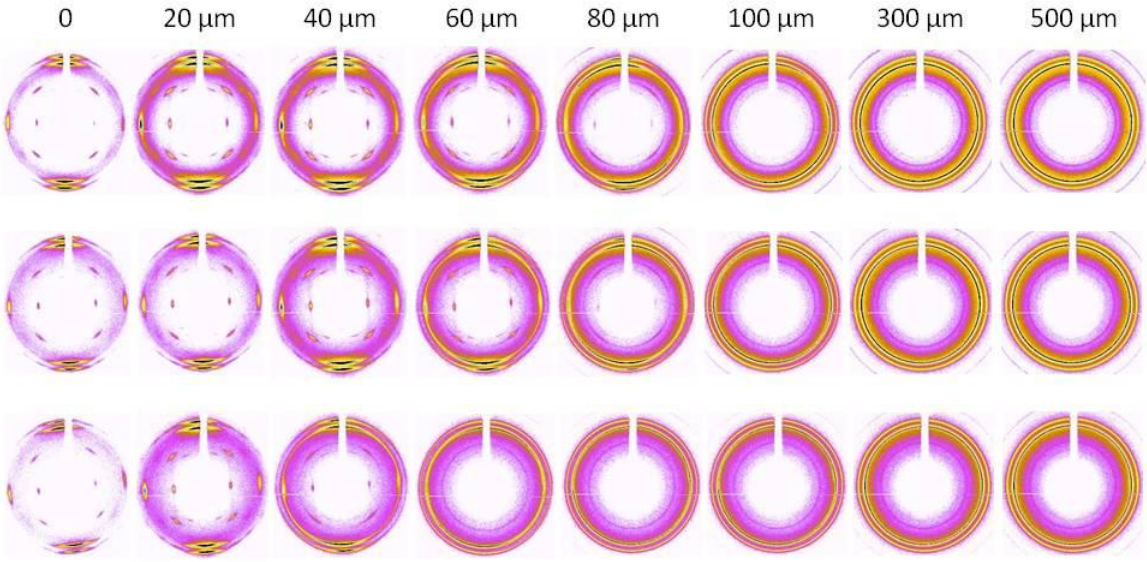

Figure 4. Selected wide-angle X-ray scattering patterns of micro-molded PCL/PVME blends (from top to bottom: 100/0, 90/10, and 70/30) recorded at different sample thickness positions before tensile deformation. The values for the distance from sample surface are indicated above each pattern. The effective *q* range of WAXS diagrams is 2.75-38.97 nm^{-1}.

Furthermore, the WAXS images taken at different sample thickness positions show typical patterns as illustrated in Figure 4. It can be seen that there exists a clear skin-core structure along the thickness of the micro-molded samples. With increasing distance from sample surface the WAXS patterns become less anisotropic and finally reach a pattern with isotropic scattering intensity distribution. The value of the degree of orientation of the lattice plane *hkl* can be derived from the azimuthal intensity distribution function $I(\mu)$ along the scattering circle by use of the Polanyi equation:[37]

$$\cos\vartheta_{hkl} = \cos\theta_{hkl}\cos\mu \qquad (2)$$

where θ_{hkl} denotes the Bragg scattering angle. This equation correlates the azimuthal angle μ along the Debye circle with the angle ϑ_{hkl} between the extensional direction and the normal vector of the lattice plane. The orientational order parameter is used as a measure for the degree of orientation in uniaxially oriented samples. It is expressed as follows[38]

$$S_{hkl} = \frac{3\langle\cos^2\vartheta_{hkl}\rangle - 1}{2} \qquad (3)$$

where $\left\langle \cos^2 \vartheta_{hkl} \right\rangle = \frac{\int_0^{\frac{\pi}{2}} I_{hkl}(\vartheta) \sin \vartheta \cos^2 \vartheta d\vartheta}{\int_0^{\frac{\pi}{2}} I_{hkl}(\vartheta) \sin \vartheta d\vartheta}$ (4)

For a perfect orientation of the lattice plane with its normal perpendicular to the stretching direction, the order parameter is S = -0.5, while for an isotropic sample in the randomly oriented state, the order parameter becomes S = 0. The azimuthal scans of the intensity distribution of the 110-reflection are given in Figure S1, and the results for the orientational order parameters of the 110-reflection are presented in Figure 5. As the distance from the edge is increased, the degree of orientation increases firstly followed by a considerable drop, and finally reaches a plateau. The reason for an initial increase in orientation is due to the fact that rapid solidification of the polymer at the edge forms a new wall where shear rate is increased as a result of a decrease in cross-sectional area of the cavity. As can be seen, the thickness of oriented skin layers is about 100 μm for all the micro-molded blends, which agrees well with the results of optical microscopy (Figure S2).

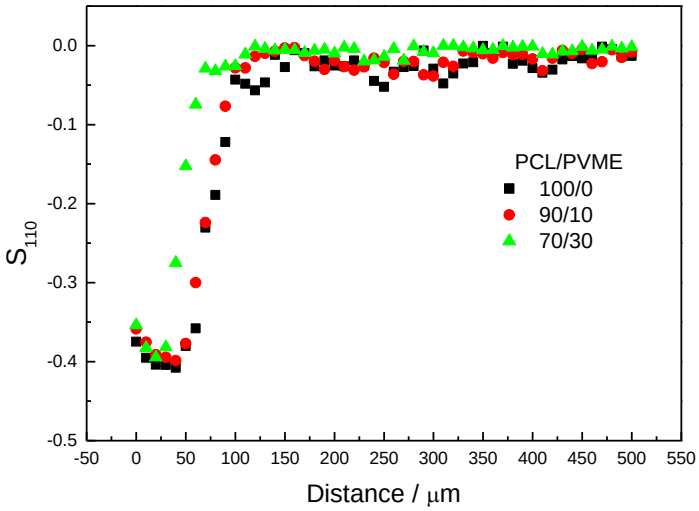

Figure 5. Evolution of the orientational order parameters associated with the 110-reflection as a function of distance from the sample surface measured for the micro-molded PCL/PVME blends.

3.2. DSC and Stress-Strain Curves. Since our main purpose is to assess the influence of the flow-oriented crystalline structure on the deformation behavior of PCL/PVME blends, we have limited our observations to one injection velocity at which a higher degree of orientation is produced. Figure 6 displays DSC heating scans of micro-molded PCL/PVME blends before tensile test. The results for the glass transition temperature and melting point as well as crystallinity are summarized in Table 1. For all the mixtures, the melting point remains essentially constant, and the glass transition temperature increases with increasing amount of PVME (T_g = -31 ^{o}C). In addition, the sample crystallinity derived from the heat of fusion decreases when the fraction of PVME gets larger. Figure 7 presents the relationship between the true stress and the true strain for all PCL/PVME

blends. It is evident that the stress decreases remarkably with increasing content of PVME, indicating that PVME molecular chains mix with the amorphous phase of PCL and thus resulting in a reduced modulus of the entangled amorphous network.

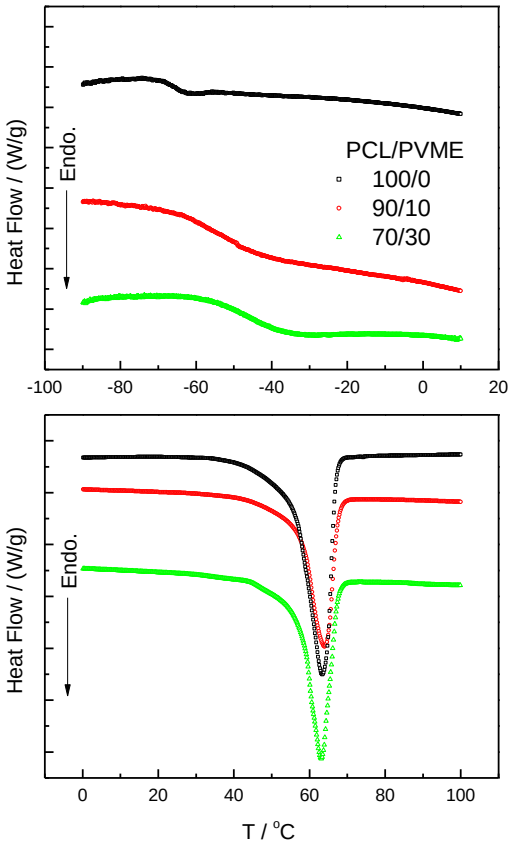

Figure 6. DSC thermograms of PCL/PVME blends measured at a heating rate of 10 K/min before tensile deformation. The samples used are micro-molded at an injection velocity of 100 mm/s.

Table 1. Thermal Properties of Samples Micro-Molded at an Injection Speed of 100 mm/s

Sample	T_g[a] / °C	T_m[b] / °C	φ_c[c]
Pure PCL	-65.17	63.63	54.34%
PCL/PVME=90/10	-52.26	63.94	48.44%
PCL/PVME=70/30	-46.31	63.17	46.98%

[a] The glass transition temperature (T_g) is derived from the midpoint of the endothermic step in the DSC heating scan. [b] The melting point (T_m) denotes the minimum of the thermogram during heating. [c] The mass fraction of crystallites with respect to the total weight of blends (φ_c) is calculated from the heat of fusion based on the melting enthalpy of hypothetical 100% crystalline PCL of 157 J/g (from ATHAS databank).

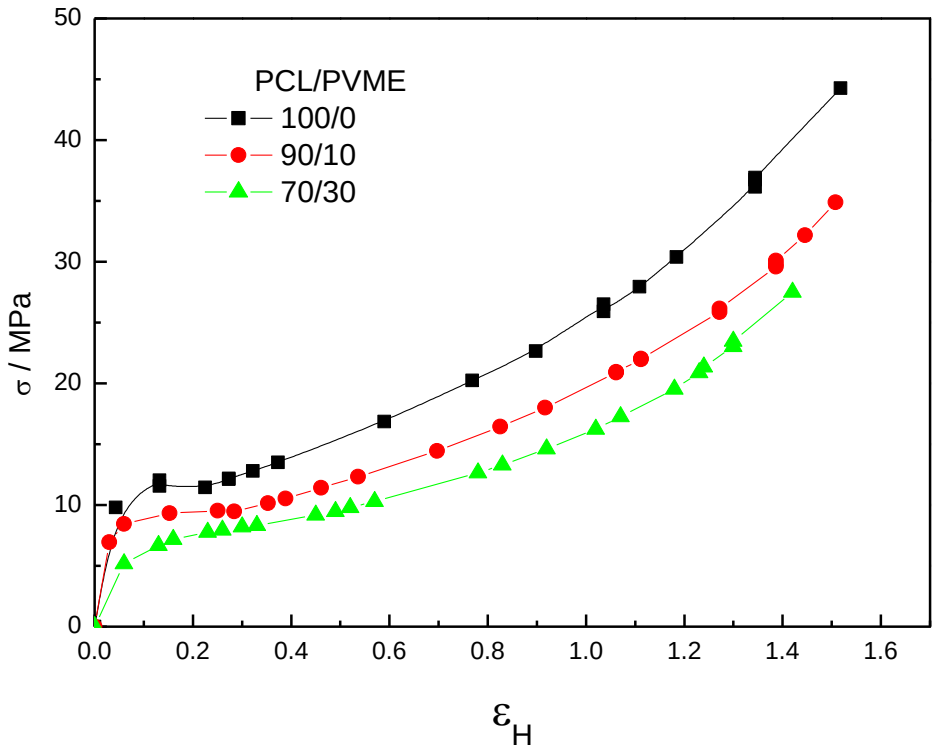

Figure 7. True stress-strain curves of micro-molded PCL/PVME blends measured during tensile deformation with a constant crosshead speed of 0.01 mm/s at room temperature.

3.3. In Situ SAXS Results. Information about changes in the lamellar structure during tensile deformation can be extracted directly from the in situ 2D SAXS patterns. Selected SAXS patterns for micro-molded PCL/PVME blends, which were deformed at room temperature to different deformation ratios, are illustrated in Figure 8.

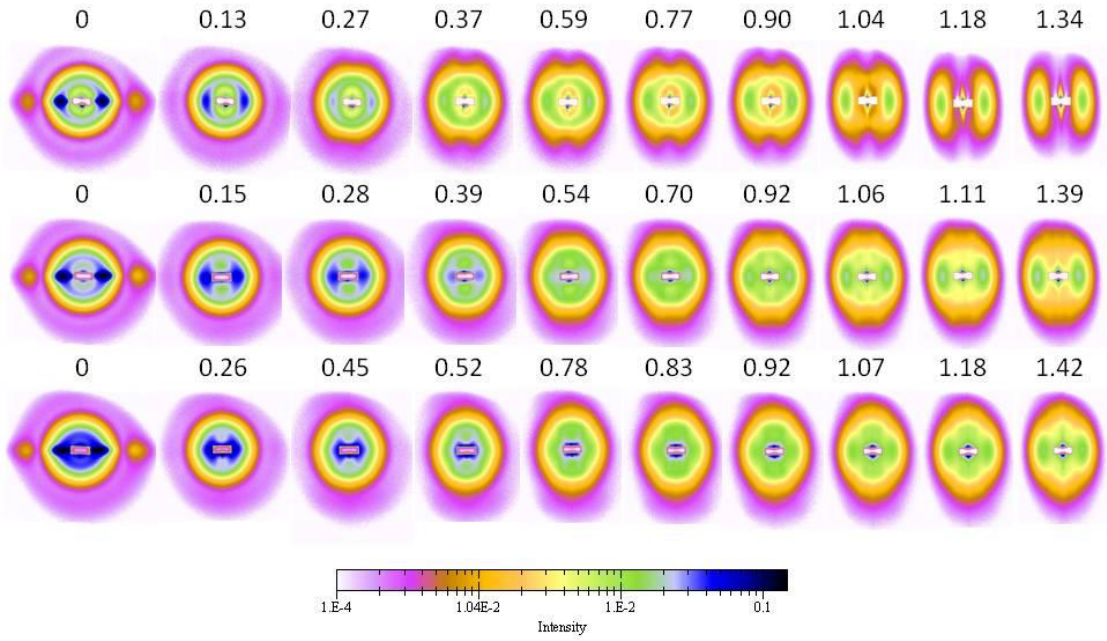

Figure 8. Selected small-angle X-ray scattering patterns of PCL/PVME blends (from top to bottom: 100/0, 90/10, and 70/30) tensile deformed at room temperature as a function of true strain. The samples used were micro-molded at an injection velocity of 100 mm/s, and the stretching direction is horizontal. The effective q range of SAXS diagrams is 0.20-1.60 nm^{-1}.

The evolution of SAXS patterns in the micro-molded blends follows a similar characteristic during stretching. As the deformation ratio increases, the SAXS patterns

transform from a scattering diagram with peaks parallel to the flow direction at small deformations to a four-point scattering diagram at moderate strains, and eventually to a highly anisotropic scattering intensity distribution with scattering peaks aligned in the meridional direction (i.e., along the stretching direction). Initially, the original scattering intensity in the meridian direction becomes weaker with increasing stretching ratio, which is caused by a destruction of crystalline lamellae with their normal along the drawing direction. Subsequently, the presence of four-point SAXS patterns is indicative of a slipping/tilting of the oriented lamellar crystallites. The observation can be explained by assuming that lamellar stacks that are inclined with respect to the macroscopic orientation direction are able to experience intralamellar slip, keeping some correlation within the stacks, while lamellae having normals both parallel with and perpendicular to the stretching direction are broken, resulting in a loss of SAXS intensity. With increasing deformation a new meridian long spacing scattering peak can be observed at a strain where the lamellar-to-fibrillar transition just sets in, yielding new lamellae with their normals parallel to the stretching direction. The effect of an introduction of PVME on the SAXS patterns and thus the microstructure of samples during tensile deformation is also derived from the data in Figure 8. Two main characteristics can be identified from the SAXS patterns. With increasing composition of PVME the original lamellar stacks can persist up to a larger strain in the deformation process. This behavior can be explained by the fact that an inclusion of PVME into the amorphous domains of PCL lowers the modulus of the amorphous phase and thus reducing the effective network stress

transferred to the crystalline skeleton. The other important feature to be noted is that a strong scattering streak passing though the beam center appears on the equator in blends with higher volume fraction of PVME after uniaxial elongation. Such a scattering behavior implies the formation of an elongated heterogeneous structure of different electron density along the stretching direction such as fibrils or cavities. However, cavitation can be ruled out in the present case because all samples show no strain whitening during stretching. If the scattering streak were due to cavities, the scattering intensity would be much stronger than that observed here. In addition, the yield stress decreases significantly with increasing concentration of PVME (as shown in Figure 7). As it turns out, plastic deformation of crystals occurs in polymers with crystals of lower plastic resistance, while cavitation occurs in polymers with crystals of higher plastic resistance.[39] Therefore, cavitation could be completely suppressed at higher volume fractions of PVME. Hence, this equatorial scattering streak can be assigned to the increased contrast between the fibrils and the interfibrillar materials, namely, the occurrence of phase separation in the tensile deformation of miscible blends, which is consistent with the results of isotropic samples at high strains.[40]

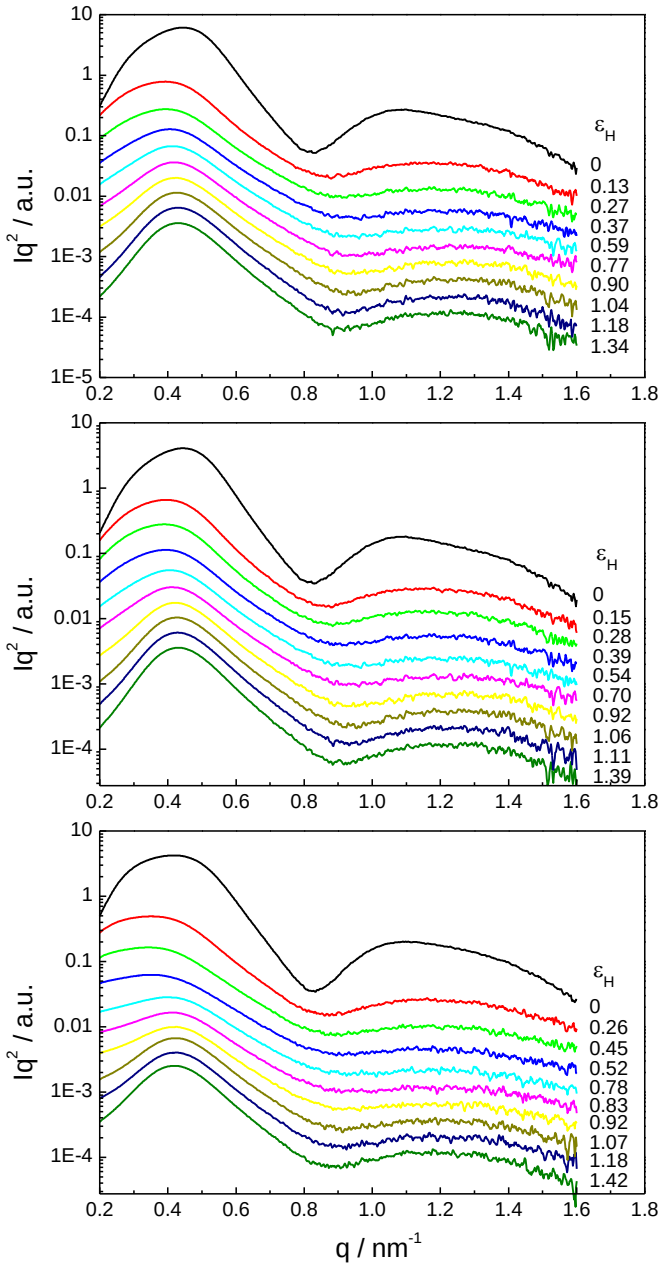

Figure 9. One-dimensional scattering intensity distribution profiles for micro-molded PCL/PVME blends (from top to bottom: 100/0, 90/10, and 70/30) taken along the stretching direction at different deformations.

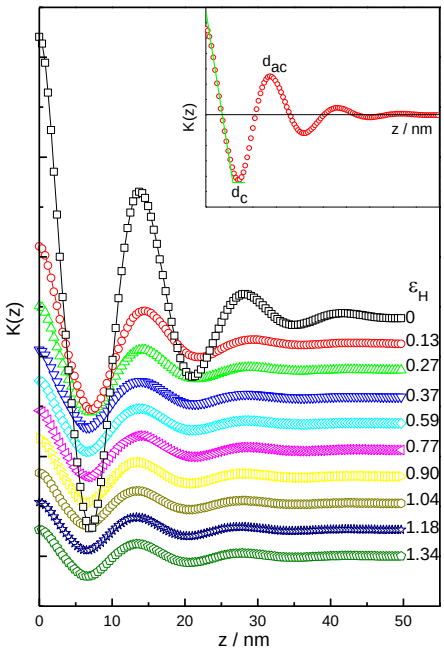

Figure 10. One-dimensional correlation functions for pure PCL taken at different deformations. The long spacing (d_{ac}) together with the average thicknesses of crystalline lamellae (d_c) and amorphous layers (d_a) can be obtained from the correlation function as illustrated in the inset diagram.

In order to elucidate the evolution of crystalline lamellae under tension, one-dimensional scattering intensity distributions along the stretching direction are considered (Figure 9). As discussed in our previous investigations, for a semiquantitative discussion of the dependence of the long spacing on the strain, the type of data treatment (Lorentz correction versus no correction) plays only a subordinate role.[26-28] Consequently, Lorentz-corrected scattering curves were applied in the present work to evaluate the microstructural parameters. The average thicknesses of the crystalline lamellae and

amorphous layers measured along the stretching direction can be derived from the one-dimensional electron density correlation function *K(z)* as follows:[41-45]

$$K(z) = \frac{\int_0^\infty I(q)q^2 \cos(qz)dq}{\int_0^\infty I(q)q^2 dq} \qquad (5)$$

where *z* is along the drawing direction. The resultant correlation functions for the pure PCL are illustrated as a function of deformation ratio in Figure 10. The inset diagram in Figure 10 demonstrates how the average thickness of the crystalline lamellae (d_c) and the long spacing (d_{ac}) are obtained. It must be mentioned that it is impossible to decide whether it is the amorphous or the crystalline thickness that is directly read out from the correlation function without prior knowledge of crystallinity values.[42] Although the crystallinity of the pure PCL sample used in the present study was higher than 0.5, the linear crystallinity (d_c/d_{ac}) should be lower than the bulk crystallinity derived from the heat of fusion, due to lower density of the amorphous phase with respect to the crystallites. Accordingly, the smaller value is assigned to the average thickness of the crystalline lamellae (d_c). The average thickness of the amorphous layers can thus be calculated with the relation $d_a = d_{ac} - d_c$.

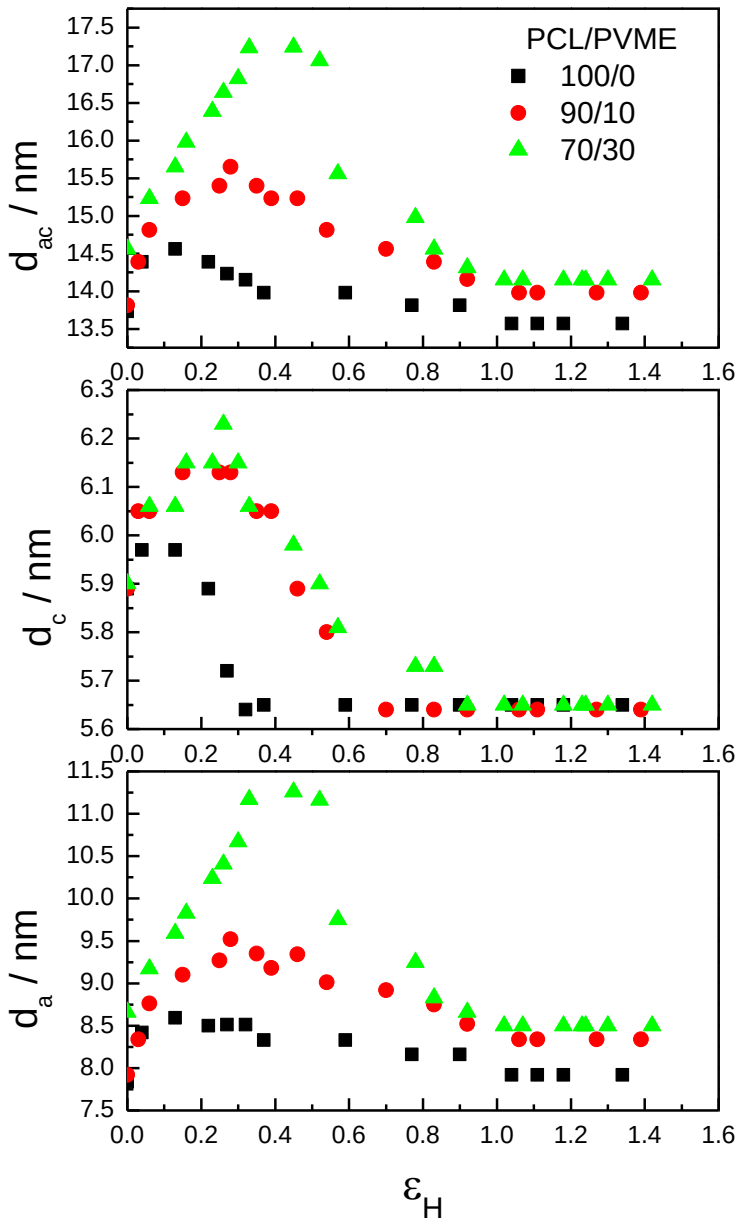

Figure 11. Evolution of the long spacing (d_{ac}) (top) together with the average thicknesses of the crystalline lamellae (d_c) (middle) and the amorphous layers (d_a) (bottom) as a function of strain measured for the micro-molded PCL/PVME blends.

Figure 11 displays the development of these parameters as a function of strain and PVME fraction during stretching. For all the blends, it becomes obvious that the long

spacing together with the average thicknesses of lamellar and amorphous regions along the stretching direction qualitatively behave in a similar manner to each other upon deformation. The values of d_{ac}, d_c, and d_a increase gradually at small deformations followed by a significant drop, and eventually level off at a critical strain. This finding is in line with the fragmentation and recrystallization process during deformation. Since the imposed drawing temperature (23 ^{o}C) was slightly lower than the mold temperature (30 ^{o}C), the recrystallization process produces lamellae that are thinner than the original ones because of the high undercooling.[46] When the amorphous compound PVME is introduced, there is a considerable increase in the long spacing for the blends in the initial stages of deformation, the extent of which depends on the proportion of PVME. This behavior is caused by readily stretching of the interlamellar amorphous layers and an accompanying slight arrangement of lamellae. In addition, it is obvious that the critical strain, at which a constant value of lamellar thickness is reached, shifts to a higher value with increasing PVME composition. This can be interpreted by assuming that the incorporated amorphous component PVME acts as an effective diluent of the entanglement density of the PCL amorphous phase thus resulting in a reduced modulus of the entangled amorphous network. Deviating from our previous results,[40] the long spacing varies with the deformation ratio and the concentration of PVME at high strains during stretching due to shrinkage of the amorphous layers to a different extent after lamellar-to-fibrillar transition. This finding can be ascribed to be the relaxation of stretched amorphous chains being accommodated by the slippage of fibrils past each other. The present results

indicate that it is easier to overcome the opposing forces imposed by chains connecting neighboring fibrils than pulling apart lamellae that are connected by a dense network of amorphous chains. The slippage is, therefore, facilitated by the weak coupling force between fibrils at high deformations, giving rise to a slight reduction in the average thickness of the amorphous layers. On the other hand, because of incorporation of the amorphous polymer PVME into the interfibrillar regions after fibrillation for the PCL/PVME blends, the interaction between adjacent fibrils becomes stronger due to the resulting jammed packing, and stretching of the blends implies tensile extension of a network of taut amorphous chains connecting adjacent fibrils. Hence, the slippage of the fibrils passing each other is limited at high elongations in the oriented PCL/PVME blends.

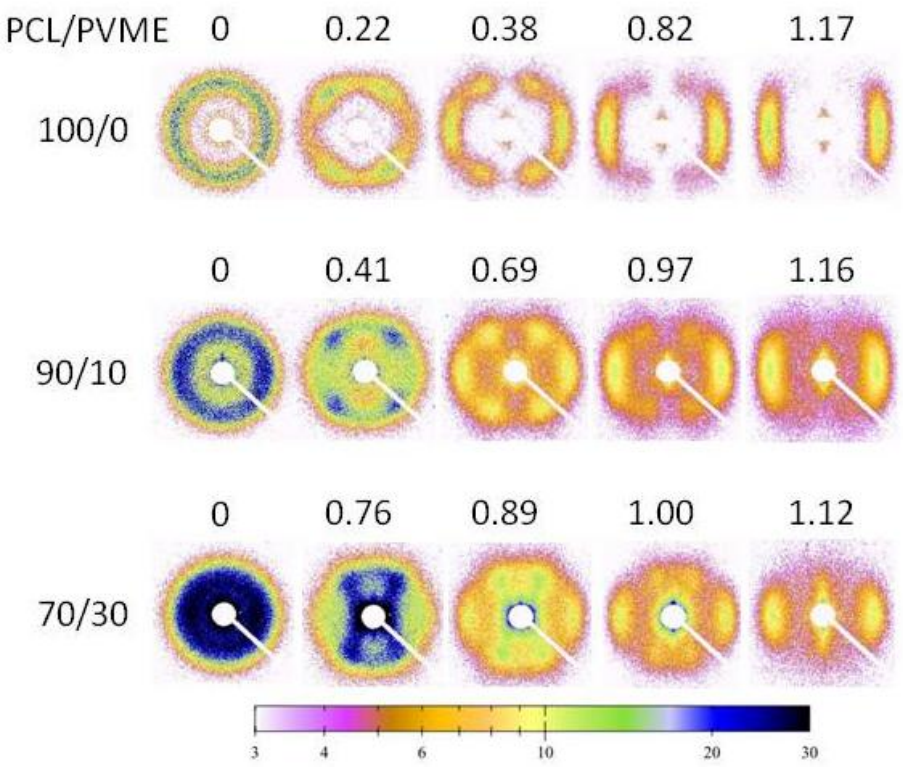

Figure 12. Selected small-angle X-ray scattering patterns of the core of micro-molded PCL/PVME blends measured as a function of true strain. The stretching direction is horizontal. The effective *q* range of SAXS diagrams is 0.11-1.20 nm^{-1}.

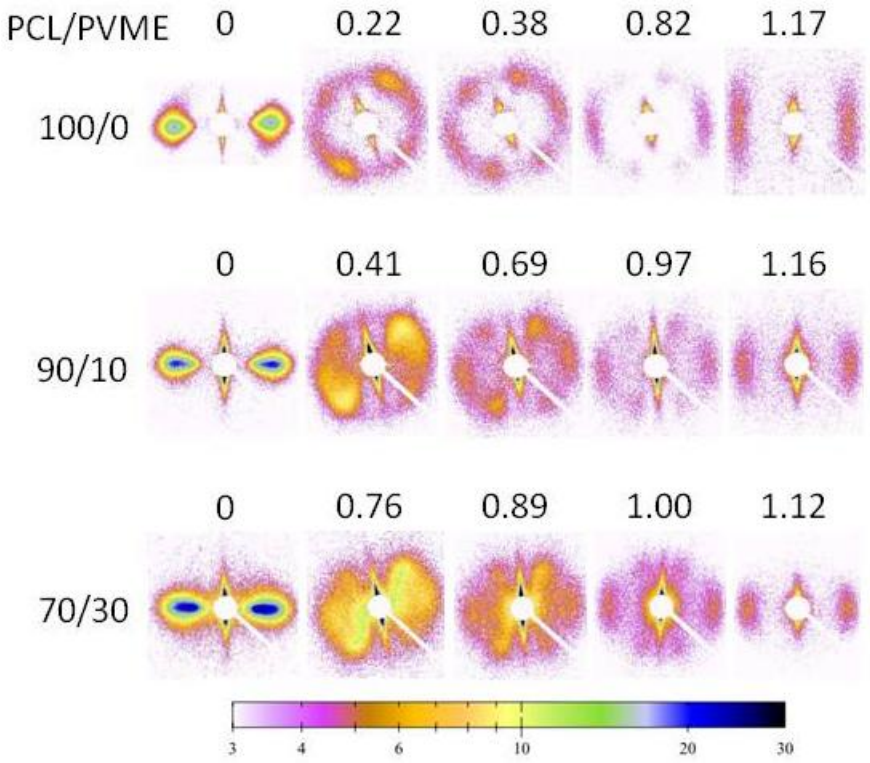

Figure 13. Selected small-angle X-ray scattering patterns of the skin layers of micro-molded PCL/PVME blends measured as a function of true strain. The stretching direction is horizontal. The effective *q* range of SAXS diagrams is 0.11-1.20 nm^{-1}.

3.4. Scanning SAXS Results. In order to clarify the deformation behavior at different positions of the micro-molded sample, the structural evolution of the core and skin layers was studied as a function of deformation ratio, respectively. Figure 12 illustrates SAXS

patterns of the core of micro-molded PCL/PVME blends during uniaxial stretching. With increasing deformation the transition from the original isotropic scattering distribution to highly anisotropic streak-like scattering patterns can be observed. The characteristics of the evolution of the microstructure in the systems during stretching follow a common scheme as discussed before for isotropic semicrystalline polymers.[27,28,40] Figure 13 presents the variation of SAXS diagrams with strain for the skin layers of micro-molded mixtures. As can be seen, the SAXS pattern shows a highly anisotropic scattering distribution prior to deformation indicating an oriented lamellar structure along the flow direction. With increasing elongation ratio the original scattering intensity along the stretching direction decreases gradually, due to a loss of the positional correlation between the crystallites in the meridian direction. Meanwhile, a two-point-like SAXS pattern appears at oblique angles with respect to the stretching direction, and the positions of these scattering peaks gradually move closer to the equator. This phenomenon can be ascribed to a slipping or tilting of the oriented lamellar crystallites. On the other hand, a pattern with two straight streaks perpendicular to the drawing direction arises at high deformations. This behavior is consistent with the previously proposed assumption of a stress-induced fragmentation and recrystallization process during stretching. When the composition of PVME is raised, there is a considerable increase in the scattering intensity before deformation reflecting that the noncrystallizable compound PVME is still included in the lamellar stacks.

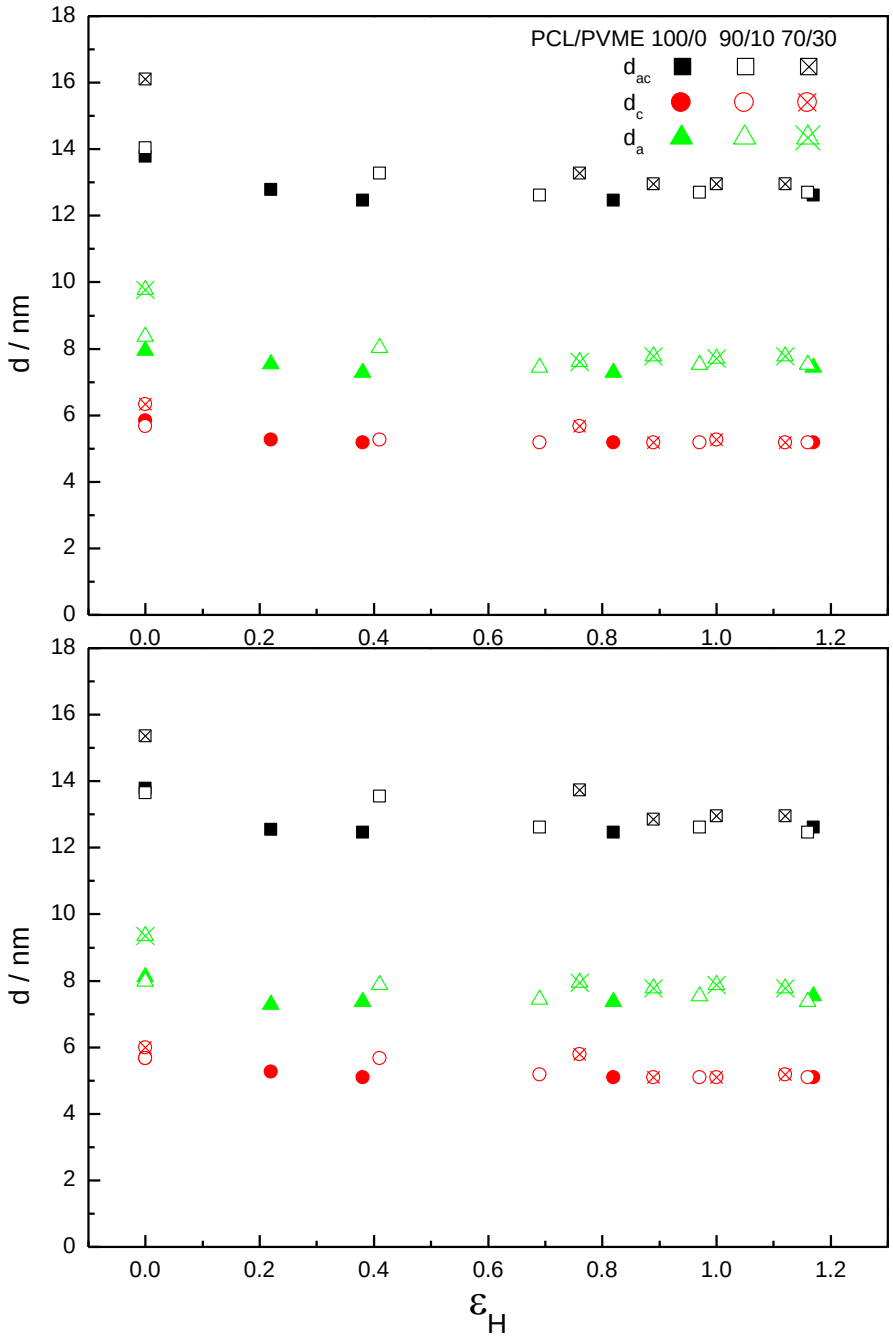

Figure 14. True-strain dependence of the long spacing (d_{ac}) together with the average thicknesses of crystalline (d_c) and amorphous regions (d_a) along the drawing direction measured for the core (top) and skin layers (bottom) of micro-molded PCL/PVME blends after uniaxial extension.

The scattering intensity distribution for stacks of lamellae was obtained by meridian scans along the stretching direction, as shown in Figure S3. The average thicknesses of the crystalline and amorphous regions as well as the long spacing measured along the drawing direction were also evaluated from SAXS data using the one-dimensional correlation function (Figure S4). The evolution of these structural parameters is presented as a function of strain in Figure 14. For both the core and skin layers, the inclusion of a noncrystallizable component of PVME does not much change the thickness of crystalline lamellae and leads mainly to a swelling of the amorphous phase of PCL before deformation. In addition, the long spacing remains essentially unchanged with strain at high stretching ratios, regardless of the concentration of PVME and the region of micro-molded sample. This behavior is distinctly different from that observed in micro-molded PCL/PVME blends as a whole. The discrepancy is attributed to the fact that the slippage of fibrils is inverted after unloading due to relaxation of the stretched chains connecting adjacent fibrils.

Based on the above observations, the structural evolution of micro-molded PCL and its miscible blends with PVME on a nanometric scale is elucidated in the process of tensile elongation, as schematically represented in Scheme 1.

Scheme 1. Schematic Representation of the Structural Evolution of the Micro-Molded PCL and Its Blends with PVME under Tensile Deformation at Room Temperature[a]

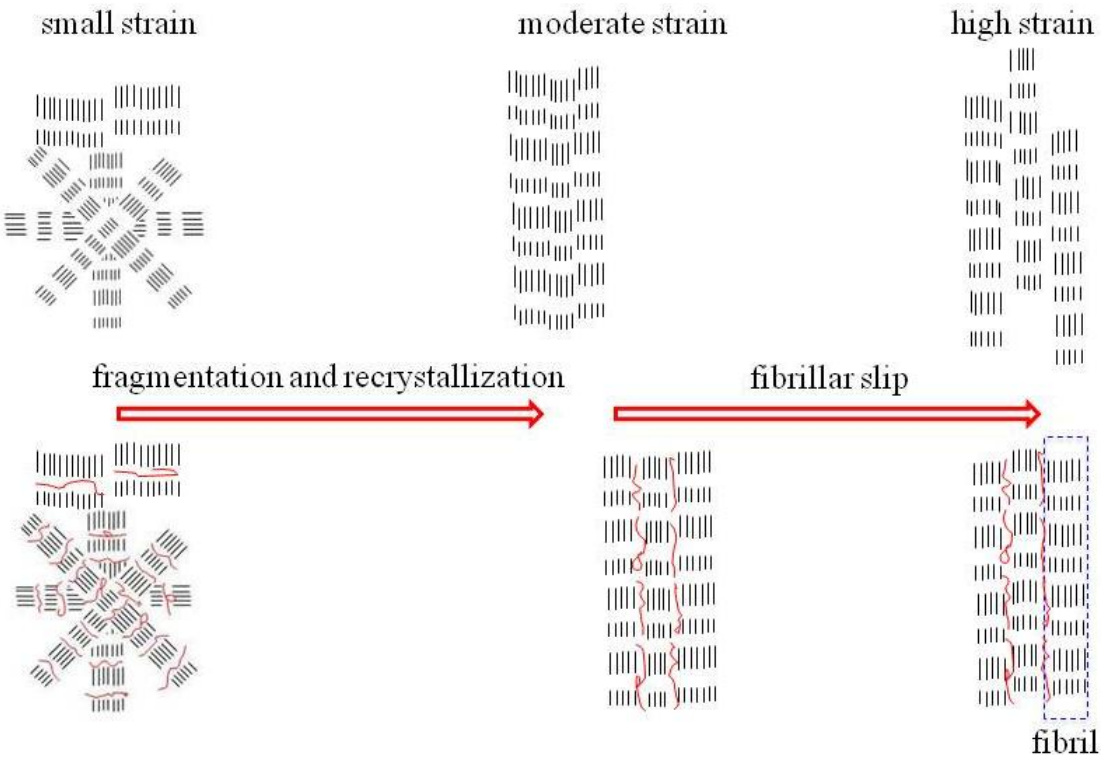

[a]The solid lines and red curves denote the PCL layer-like lamellar crystallites and PVME amorphous polymeric chains, respectively. The stretching direction is vertical.

4. Conclusions

The influence of micro-molding on the microstructural evolution in the miscible blends of PCL with the amorphous compound PVME was investigated using in situ synchrotron SAXS and scanning SAXS experiments. The role of the entangled amorphous phase and the deformation mechanisms of the oriented PCL/PVME blends were identified in the tensile deformation process. With the progress of uniaxial extension, crystal block slips within the crystalline lamellae were triggered at small elongations, whereas a stress-induced fragmentation of the original lamellae and recrystallization of the freed

polymeric segments along the stretching direction occurred at a critical strain where the average thickness of the crystallites remains essentially constant. It is evident that the value of the critical strain at which the lamellar to fibrillar transition just sets in is strongly dependent on the content of PVME, due to an enhanced mobility of the amorphous phase and, therefore, a reduced modulus of the entangled amorphous network upon addition of the noncrystallizable component PVME. In addition, the slippage of the fibrils was activated at high deformations, resulting in a small decrease of the average thickness of the amorphous layers. As a consequence of phase separation induced by tensile deformation in the miscible PCL/PVME blends, the resulting jammed packing of the fibrils makes it more difficult for the lamellae stacks to reconfigure themselves at large strains compared to the pure PCL.

Acknowledgments

We acknowledge financial support from National Natural Science Foundation of China (21204088 and 21134006). This work is within the framework of the RCUK/EPSRC Science Bridges China project of UK-China Advanced Materials Research Institute (AMRI).

References

(1) Strobl, G. *The Physics of Polymers,* 2nd ed.; Springer: Berlin, Germany, 1997.

(2) Schultz, J. M. *Polymer Materials Science;* Academic Press: Englewood Cliffs, NJ, 1974.

(3) Schrauwen, B. A. G.; Breemen, L. C. A. V.; Spoelstra, A. B.; Govaert, L. E.; Peters, G. W. M.; Meijer, H. E. H. *Macromolecules* **2004,** *37*, 8618.

(4) Kantz, M. R.; Newman, H. D.; Stigale, F. H. *J. Appl. Polym. Sci.* **1972,** *16*, 1249.

(5) Zipper, P.; Jánosi, A.; Wrentschur, E.; Abuja, P. M. *J. Appl. Crystallogr.* **1991,** *24*, 702.

(6) Zipper, P.; Jánosi, A.; Geymayer, W.; Ingolic, E.; Fleischmann, E. *Polym. Eng. Sci.* **1996,** *36*, 467.

(7) Zhong, G. J.; Li, L. B.; Mendes, E.; Byelov, D.; Fu, Q.; Li, Z. M. *Macromolecules* **2006,** *39*, 6771.

(8) Yang, H. R.; Lei, J.; Li, L. B.; Fu, Q.; Li, Z. M. *Macromolecules* **2012,** *45*, 6600.

(9) Ning, N. Y.; Luo, F.; Pan, B. F.; Zhang, Q.; Wang, K.; Fu, Q. *Macromolecules* **2007,** *40*, 8533.

(10) Wang, K.; Chen, F.; Zhang, Q.; Fu, Q. *Polymer* **2008,** *49*, 4745.

(11) Failla, M. D.; Mandelkern, L. *Macromolecules* **1993,** *26*, 7167.

(12) Bartczak, Z. *Macromolecules* **2005,** *38*, 7702.

(13) Kennedy, M. A.; Peacock, A. J.; Mandelkern, L. *Macromolecules* **1994,** *27*, 5297.

(14) Wang, Y.; Xiao, Y.; Zhang, Q.; Gao, X. L.; Fu, Q. *Polymer* **2003,** *44*, 1469.

(15) Tang, Y. J.; Jiang, Z. Y.; Men, Y. F.; An, L. J.; Enderle, H. F.; Lilge, D.; Roth, S. V.; Gehrke, R.; Rieger, J. *Polymer* **2007**, *48*, 5125.

(16) Shinohara, Y.; Yamazoe, K.; Sakurai, T.; Kimata, S.; Maruyama, T.; Amemiya, Y. *Macromolecules* **2012,** *45*, 1398.

(17) Zhu, P. W.; Tung, J.; Phillips, A.; Edward, G. *Macromolecules* **2006,** *39*, 1821.

(18) Liu, P.; White, K. L.; Sugiyama, H.; Xi, J.; Higuchi, T.; Hoshino, T.; Ishige, R.; Jinnai, H.; Takahara, A.; Sue, H. J. *Macromolecules* **2013,** *46*, 463.

(19) Ségui, R. *e-Polym.* **2007**, *no. 032*.

(20) Butler, M. F.; Donald, A. M.; Bras, W.; Mant, G. R.; Derbyshire, G. E.; Ryan, A. J. *Macromolecules* **1995,** *28*, 6383.

(21) Pawlak, A.; Galeski, A. *Macromolecules* **2005,** *38*, 9688.

(22) Ran, S. F.; Wang, Z. G.; Burger, C.; Chu, B.; Hsiao, B. S. *Macromolecules* **2002,** *35*, 10102.

(23) Galeski, A.; Bartczak, Z.; Argon, A. S.; Cohen, R. E. *Macromolecules* **1992**, *25*, 5705.

(24) Men, Y.; Strobl, G. *Macromolecules* **2003**, *36*, 1889.

(25) Men, Y. F.; Rieger, J.; Strobl, G. *Phys. Rev. Lett.* **2003,** *91*, 095502.

(26) Jiang, Z. Y.; Tang, Y. J.; Rieger, J.; Enderle, H. F.; Lilge, D.; Roth, S. V.; Gehrke, R.; Heckmann, W.; Men, Y. F. *Macromolecules* **2010**, *43*, 4727.

(27) Jiang, Z. Y.; Tang, Y. J.; Men, Y. F.; Enderle, H. F.; Lilge, D.; Roth, S. V.; Gehrke, R.; Rieger, J. *Macromolecules* **2007**, *40*, 7263.

(28) Jiang, Z. Y.; Tang, Y. J.; Rieger, J.; Enderle, H. F.; Lilge, D.; Roth, S. V.; Gehrke, R.; Wu, Z.; Li, Z.; Men, Y. F. *Polymer* **2009**, *50*, 4101.

(29) Bisso, G..; Casarino, P.; Pedemonte, E. *Macromol. Chem. Phys.* **1999**, *200*, 376.

(30) Li, W.; Prud'homme, R. E. *Polymer* **1994**, *35*, 3260.

(31) Chiu, S. C.; Smith, T. G.. *J. Appl. Polym. Sci.* **1984**, *29*, 1797.

(32) Stein, R. S.; Khambatta, F. B.; Warner, F. P.; Russell, T.; Escala, A.; Balizer, E. *J. Polym. Sci., Polym. Symp.* **1978**, *63*, 313.

(33) Russell, T. P.; Stein, R. S. *J. Polym. Sci., Polym. Phys. Ed.* **1983**, *21*, 999.

(34) Zhao, Y.; Keroack, D.; Prud'homme, R. E. *Macromolecules* **1999**, *32*, 1218.

(35) Keroack, D.; Zhao, Y.; Prud'homme, R. E. *Polymer* **1998**, *40*, 243.

(36) Denny, R. C. *Fibre Diffr. Rev.* **1996**, *5*, 24.

(37) Polanyi, M. *Z. Phys.* **1921**, *7*, 149.

(38) Hermanns, P.; Platzek, P. *Kolloid Z.* **1939**, *88*, 68.

(39) Pawlak, A.; Galeski, A. *Macromolecules* **2005,** *38*, 9688.

(40) Jiang, Z. Y.; Fu, L. L.; Sun, Y. Y.; Li, X. H.; Men, Y. F. *Macromolecules* **2011,** *44*, 7062.

(41) Stribeck, N. *X-ray Scattering of Soft Matter;* Springer: Heidelberg, 2007.

(42) Glatter, O.; Kratky, O. *Small-Angle X-ray Scattering*; Academic Press: London, UK, 1982.

(43) Murthy, N. S.; Bednarczyk, C.; Moore, R. A. F.; Grubb, D. T. *J. Polym. Sci. Polym. Phys.* **1996**, *34*, 821.

(44) Strobl, G.; Schneider, M. J. *J. Polym. Sci. Polym. Phys.* **1980**, *18*, 1343.

(45) Strobl, G.; Schneider, M. J.; Voigt-Martin, I. G. *J. Polym. Sci. Polym. Phys.* **1980**, *18*, 1361.

(46) Peterlin, A.; Balta-Calleja, F. J. *Kolloid Z. & Z. Polym.* **1970,** *242*, 1093.

For Table of Contents Use Only

Tensile Deformation of Oriented Poly(ε-caprolactone) and Its Miscible Blends with Poly(vinyl methyl ether)

Zhiyong Jiang[1,], Yaotao Wang[1], Lianlian Fu[1], Ben Whiteside[2], John Wyborn[2], Keith Norris[2], Zhonghua Wu[3], Phil Coates[2,*], and Yongfeng Men[1]*